International Journal of Thermal Sciences 75 (2014) 140–152

Contents lists available at ScienceDirect

International Journal of Thermal Sciences

journal homepage: www.elsevier.com/locate/ijts

Local heat transfer measurement and thermo-fluid characterization of a pulsating heat pipe

Mauro Mameli [a,*], Marco Marengo [a], Sameer Khandekar [b]

[a] University of Bergamo, Department of Industrial Engineering, viale Marconi 5, 24044 Dalmine, Italy
[b] Indian Institute of Technology Kanpur, 208016 Kanpur, UP, India

ARTICLE INFO

Article history:
Received 21 February 2013
Received in revised form
18 July 2013
Accepted 29 July 2013
Available online

Keywords:
Pulsating Heat Pipes
Local heat transfer
Pressure variation
Flow patterns

ABSTRACT

A compact Closed Loop Pulsating Heat Pipe (CLPHP), filled with ethanol (65% v/v), made of four transparent glass tubes forming the adiabatic section and connected with copper U-turns in the evaporator and condenser sections respectively, is designed in order to perform comprehensive thermal-hydraulic performance investigation. Local heat transfer coefficient is estimated by measurement of tube wall and internal fluid temperatures in the evaporator section. Simultaneously, fluid pressure oscillations are recorded together with the corresponding flow patterns. The thermal performances are measured for different heat input levels and global orientation of the device with respect to gravity. One exploratory test is also done with azeotropic mixture of ethanol and water. Results show that a stable device operation is achieved (i.e. evaporator wall temperatures can reach a pseudo-steady-state) only when a circulating flow mode is established superimposed on local pulsating flow. The heat transfer performance strongly depends on the heat input level and the inclination angle, which, in turn, also affect the ensuing flow pattern. The spectral analysis of the pressure signal reveals that even during the stable performance regimes, characteristic fluid oscillation frequencies are not uniquely recognizable. Equivalent thermal conductivities of the order of 10–15 times that of pure copper are achieved. Due to small number of turns horizontal mode operation is not feasible. Preliminary results indicate that filling azeotropic mixture of ethanol and water as working fluid does not alter the thermal performance as compared to pure ethanol case.

1. Introduction

The present industry demand of high heat transfer capability coupled with relatively cheaper component costs catalyses evolution of novel two-phase passive devices. A conceptually similar to the Pulsating Heat Pipe (PHP), was introduced by Smyrnov and Savchenkov in 1971 [1]. More practical design variation of this concept, from an engineering stand-point, was proposed in the early 90s by Akachi [2,3], which subsequent fuelled several investigations to better understand this device (as summarized in Refs. [4,5]). In contemporary times too, the qualitative, as well as quantitative investigations of several design variants of Pulsating or Oscillating Heat Pipes, for potential passive thermal management applications in nuclear, defense and space are emerging at a rapid pace; this has indeed become one of the most interesting and vibrant fields of investigation. The PHP design variants being proposed and studied have the potential to meet all the present and possibly future specific requirements from electronics cooling [6,7], heat recovery [8,9] and passive cooling of reactor containments, to name a few.

A PHP usually consists of a copper capillary tube bended in a serpentine-shape closed loop (CLPHP), evacuated from within and partially filled with a working fluid, typically in its liquid-phase. As the filling volume of the fluid is less than the total internal volume of the PHP tube, the liquid-phase and vapor-phase co-exist inside the tube in the form of alternating liquid plugs and vapor bubbles, typically as a Taylor bubble train. The capillary tube diameter is chosen in such a manner that surface tension dominates over gravity forces, resulting in no bulk stratification of the phases. During heat transfer operation, one end of the serpentine tube bundle receives heat (acting as an evaporator) while the other end is kept at a lower temperature (acting as a condenser). Heating causes the thin liquid film surrounding the vapor bubbles to evaporate; bubbles thus expand and push the adjacent Taylor bubble train towards the condenser zone, where heat gets rejected to the cold source. The shrinking of vapor bubbles in the condenser

* Corresponding author. Tel.: +39 (0)352052068; fax: +39 (0)352052077.
E-mail addresses: mauro.mameli@unibg.it, mcjmameli@gmail.com (M. Mameli).

1290-0729/$ – see front matter © 2013 Elsevier Masson SAS. All rights reserved.
http://dx.doi.org/10.1016/j.ijthermalsci.2013.07.025

Nomenclature

Variables

A	area [m^2]
d	diameter [m]
EF	enhancement factor [−]
$\tilde{h}$	convective heat transfer coefficient [W/m^2 K]
k	thermal conductivity [W/m K]
L	length [m]
n	number of parallel channels [−]
$\dot{Q}$	heat power [W]
q''	heat flux [W/cm^2]
R	thermal resistance [K/W]
T	temperature [K]

Subscripts

cr	cross-section
ev	evaporator
eq	equivalent
max	maximum
out	outer
s	substrate
tot	total
w	wall
$w–f$	wall to fluid
∞	cooling medium

also provides additional motive force for the working fluid. Thus, a self-sustained thermally driven oscillating flow is set up due to the applied temperature difference, leading to enhanced passive thermal transport.

The subtle complexity of the internal thermo-fluidic behavior of the oscillating/pulsating two-phase flow is indeed quite unique, offering both opportunities and challenges for fundamental research outlook on passive two-phase transport phenomena. Design rules need to emerge from these efforts so that challenging engineering targets in the field of passive thermal management may be achieved. Paucity of design rules and lack of clarity in the fundamental operational characteristics of this intriguing system has been the major thrust of many experimental programs and supporting modeling efforts in the recent past. While most researchers have focused on the experimental study to understand the working principle of CLPHPs and delineate its driving parameters, some modest beginning has also commenced on the mathematical modeling front [10,11]. However, modeling at this stage is highly simplistic with gross assumptions. This is because all the nuances of the underlying physics of the PHP operation are still not clear and requires more experimental efforts.

Maezawa and Gi [12] investigated the temperature oscillations for PHPs operated in several heat modes (bottom heated, horizontal, top heated), two different tube diameters (1 mm and 2 mm in inner diameter) and two working fluids (water and R142b) and concluded that the random factor in the chaotic internal dynamics increases with the heat input level. Detailed flow visualization was conducted by Tong et al. [13] in a glass CLPHP: bubble nucleation and coalescence, internal two-phase flow patterns and directions were described. It was showed that the meanderings turns, uneven distribution of liquid plugs and vapor bubbles and non-concurrent boiling at the evaporator, contributed to the driving and restoring force for fluid oscillation and circulation. Kim et al. [14] performed a similar study on a flat brass plate with engraved capillary channels covered with a transparent acryl plate and reported that the liquid film surrounding the vapor plugs was approximately about 100 μm thick. They showed that the flow pattern in the evaporator region may change from capillary slug flow to a pseudo-slug flow resembling intermittent annular flow. Charoensawan et al. [15] and Khandekar et al. [16] have performed both thermal characterization and visualization of a wide number of PHP systems providing critical information on the parameter dependency of their thermal performances. It was shown that the internal diameter of the PHP tube/channels, as well as the global orientation of the devise with respect to gravity, affects the heat throughput. To overcome the effect of gravity on the thermal performance, a minimum number of serpentine turns coupled with a minimum radial heat flux are essential. Khandekar et al. [17] generated valuable information by showing the effect of different fluids, filling ratios and inclination angles on the thermal performance of PHPs. Subsequently, they also tested and characterized a single capillary loop, the primary building block of a PHP [18]. It was experimentally demonstrated that even such a simple loop exhibits multiple quasi-steady-states, which is directly correlated to the type of flow pattern inside the system [19]. Yang et al. [20] have investigated the operational limits of CLPHP and found that depending on the inner tube diameter, the minimum thermal resistance and maximum heat load are obtained when the filling ratio is between 0.4 and 0.6.

Recently Lips et al. [21] conducted several tests on a single liquid–vapor meniscus located inside a straight capillary tube which was made to oscillate by (i) adiabatically, only due to mechanical forces, and (ii) thermal gradients imposed on the length of the tube. The adiabatic experiments focused on the importance of the asymmetry between the advancing and receding contact angle during the oscillation of the meniscus. The non-adiabatic experiments showed that at low heat flux, the flow gets disturbed by bubble nucleation process, while, at a high heat flux, the main heat transfer mechanism is thin film evaporation. Both situations lead to considerable change in the thermal-hydraulic behavior. Yoon et al. [22] determined the volume fraction of the liquid-phase in different portions of the PHP tube by using neutron imaging technique. The results showed that the liquid volume fraction was always less than 2.5% in the evaporator and greater than 80% in the condenser zone.

As stated in the review by Zhang and Faghri [23] so also by others [4,5], most research efforts have been dedicated to explain the working principle of PHPs. However, a comprehensive theory of operation and a reliable database or tools for the design of PHPs still remain unrealized. Nevertheless, as the device is fully thermally driven, passive, cheap, versatile and relatively easier to build, the prospects of such systems for potential applications are too promising to be ignored.

In this background, the present work describes the complete thermo-fluid dynamic investigation on a CLPHP with four parallel transparent branches, where the fluid pressure as well as the fluid temperature are recorded, by means of a pressure transducer and two thermocouples integrated inside the tube, respectively. The local measurement of the two-phase flow temperature, together with the wall temperature at the same location and the heat input flux, provides an unprecedented estimate of the local heat transfer coefficient in a chaotic flow boiling process. Start-up fluxes as well as critical heat fluxes are monitored; the effect of heat input level, the inclination angle and the working fluid on the flow pattern and on the thermal performance are analyzed and discussed. Finally, the frequency analysis on the fluid pressure signal is performed.

2. Experimental apparatus

Recognizing the string thermo-hydrodynamic coupling inside the PHP, the set-up is designed to perform parametric investigations as well as simultaneous flow visualization. Although clearly inspired by the work of Khandekar et al. [19], the geometry of the present CLPHP is conceived specifically to avoid the occurrence of multiple-steady-states. The presence of three U-turns and four parallel channels increases the level of internal flow perturbations, thereby diminishing the probability of phase recoiling and consequent complete stopover of the fluid motion. Such a stopover occurs in a single-turn device [18].

> "The actual geometry has been chosen in between a single-loop PHP and a multi-turn PHP in order to provide necessary contribution to the available literature so as to better address the unsolved issue related to the effect of the number turns"

Fig. 1 shows an exploded view of the experimental test-cell. The tubes in the evaporator and in the condenser sections are made of copper in order to minimize the thermal resistance between the tube and the heat input/output zones, while the straight tubes in the adiabatic section are made of borosilicate glass for the purpose of visualization. All tubes have 4.0 mm O.D. and 2.0 mm I.D.; a smaller copper tube (3 mm O.D., 2 mm I.D.) is brazed on the main tube of the condenser section in order to connect the vacuum/filling valve (M/s Upchurch Scientific®). A pressure transducer (Swagelok®, PTI-S-AC5-12AS) is plugged in the left external branch of the adiabatic section by means of a T-connector (Swagelok®). The copper tubes in the condenser section are connected to the glass tubes simply by fitting a silicon tube (5 mm O.D., 3 mm I.D.). This approach is not suitable for the copper/glass connections in the evaporator zone due to the higher temperatures likely to appear in that zone. For this side therefore, a copper joint is brazed at each end of the U-turns; high temperature proof polymeric resin is filled in the remaining gap between the copper fitting and the glass tube (Fig. 2).

As the number of turns of the present PHP is rather small, orientation is expected to affect the thermal performance. Therefore, the apparatus is mounted on a tiltable frame facilitating global inclination of the set-up at any orientation with gravity. PC-based thermocouple data acquisition system (National Instruments® – NI-9211module connected to NI-cDAQ-9172chassis) has been used. The current output of the pressure transducer is connected to NI-9213® module combined with an NI-USB-9162® chassis via a 1 Ω standard reference resistance. As the characteristic frequency range of the internal PHP oscillating phenomena is expected to be 0.1 and 3 Hz based on the indications available in the literature [19,21,23], a minimum DAQ sample rate of 6.0 Hz is chosen to satisfy the Nyquist criterion.

2.1. Evaporator section

Two symmetric copper plates (100 mm × 40 mm × 3 mm) are each engraved with semi-circular cross-section channels in order to embed the copper PHP U-turns. The main novelty of the present set-up is the arrangement for measuring the local heat transfer coefficient inside the evaporator PHP tube. To achieve this, local fluid measurement is necessary inside the PHP copper tube. A 1.0 mm blind hole is drilled at the top of the curvature of the two copper U-turns in the evaporator section and two thermocouples (Omega®, K type, bead dimension of 0.3 mm, accuracy ±0.2 °C after calibration), are located inside the tube through the hole and fixed with high temperature-resistant thermal cement (Omega®), as shown in Fig. 3.

Proper thermal contact between the PHP U-turns and the evaporator copper plates is obtained using a high conductive silver-based thermal paste (RS components®) paste. Six thermocouples are located on the external tube wall by means of small square channels milled on the evaporator copper plates. The assembly of

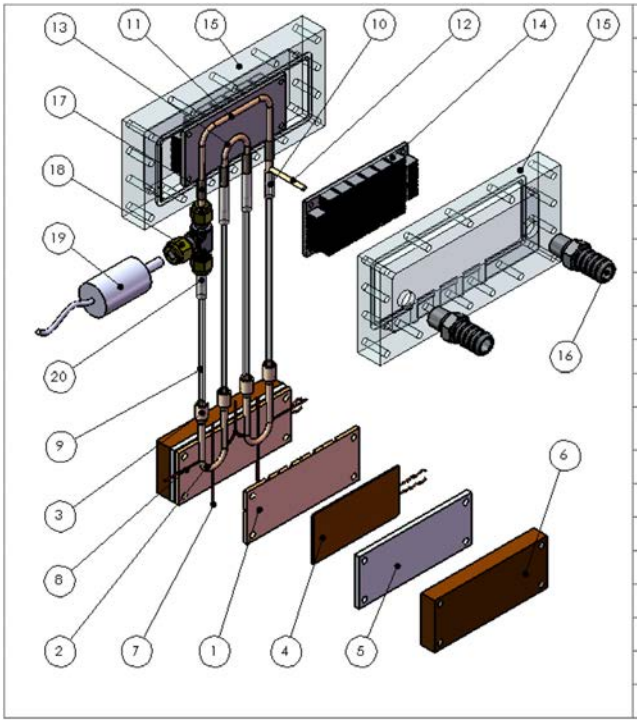

N°	ITEM
1	Evap. copper plate
2	Evap. copper U-turns
3	Copper joint
4	Heater
5	Mica sheet
6	Bakelite back plate
7	TC fluid side
8	TC wall side
9	Glass tube
10	Silicon joint
11	Condenser tube
12	Branch (vacuum/filling)
13	Cond. copper tube
14	Heat sink
15	Cooler shell
16	Cooler connector
17	Silicon seal
18	T-junction
19	Pressure transducer
20	Copper fitting

Fig. 1. Exploded view of the Closed Loop Pulsating Heat Pipe test-cell.

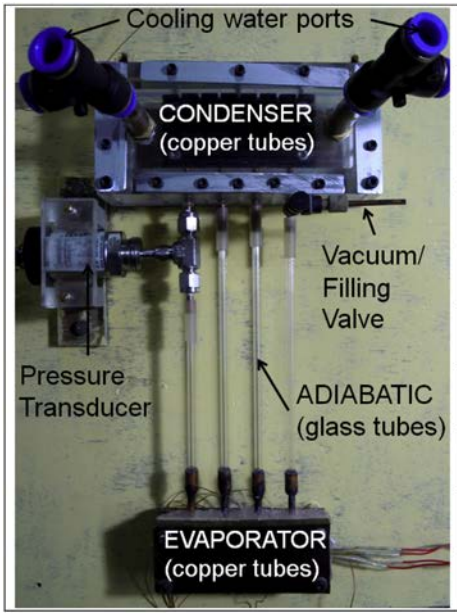

MAIN FEATURES	
Working fluid	ethanol
Tube material	copper
Tube I.D.	2 [mm]
Tube O.D.	4 [mm]
Evapaporator length	25 [mm]
Condenser length	35 [mm]
Adiabatic length	202 [mm]
Filling ratio	0.65 [-]
Cooling water temperature	15 [°C]

Fig. 2. Photograph of the pulsating heat pipe test-cell; the table alongside shows the detail of the tube geometry, materials and the experimental conditions.

the two plates and the U-turns forms the evaporator copper block. Two flat flexible heaters (Minco®, HR5383R10.7L12B) are placed at each side of the evaporator block for providing the necessary heat input. Insulation is provided by two Mica fiber sheets (thickness: 3 mm) and two Bakelite® backing plates (each of thickness 12 mm). Electric power is provided to the heaters by means of a dual tracking power supply (Scientific®) with DC current output (0–30 V, 0–3 A).

2.2. Condenser and adiabatic section

The copper tubes located in the condenser section are embedded into a finned heat sink (Alpha®, UB90-15B) with the same procedure described for the evaporator; the condenser is overdesigned such that the heat releasing surface is enhanced by a factor 35 with respect to the smooth tubes so as to dissipate the whole heat throughput by means of external liquid cooling. The condenser-block itself fits into a custom poly-carbonate shell made of two transparent plates where the cooling water is kept at 15 °C and circulated by means of a thermal circulation bath (Haake®, DC-10, K20); inlet and outlet temperature are monitored by means of two K-thermocouples.

The adiabatic zone is made of four straight borosilicate glass tubes for the purpose of fluid visualization. To clearly distinguish the two phases when internal flow oscillations take place, a white screen with four black stripes (one for each transparent tube) is placed behind the adiabatic section. Fluid motion and flow patterns are captured with a camera (Nikon®, model: Dx40) in a 100 mm × 100 mm window just above the evaporator section. Fig. 4 shows the typical liquid slugs and vapor plug distribution after the filling procedure.

2.3. Experimental methodology and control parameters

Every experiment is carried on with the following procedure.

a) Preliminary operations:
   1) The peripheral devices (PC, DAQ, thermal bath, power supplies) are switched on. Power supply is in stand-by (no electric power is provided to the heater yet). The thermal

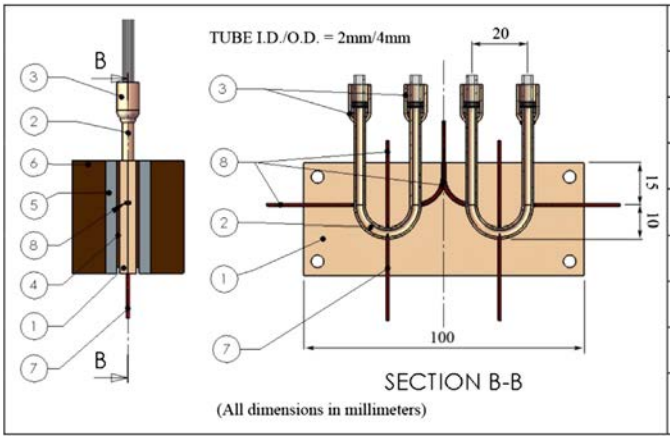

N°	ITEM
1	Copper plate
2	Copper U-turns
3	Copper joint
4	Heater
5	Mica sheet
6	Bakelite back plate
7	TC-fluid side
8	TC-wall side

Fig. 3. Detail and section of the evaporator block.

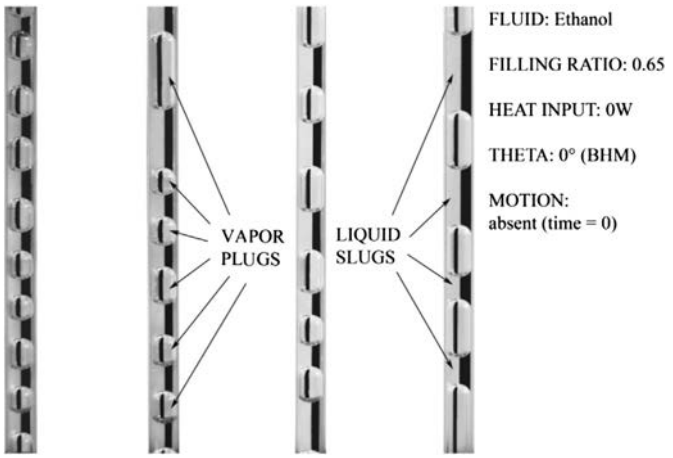

Fig. 4. Typical photographs of the adiabatic section obtained by the camera; the two phases are clearly distinguished by the black and white background screen due to the difference in the refractive index of the two phases.

bath is activated in order to reach a steady cooling water temperature.

2) The PHP is connected to an ultra-high diffusion-molecular vacuum combo system (Varian®, DS-102, Varian®, V70) through the micro-metering filling valve; when the desired vacuum level of 0.01 Pa is reached, the valve is closed and the vacuum stability inside the PHP is checked again by means of the pressure transducer located at the left external branch of the adiabatic section.
3) A 5 ml syringe is filled with working fluid and it is connected to the vacuum/filling valve by mean of a silicon tube. The syringe piston is then removed and the air trapped in the tube connection is eliminated by tapping the tube. The filling valve is slowly opened in such a way that the working fluid can enter the PHP thanks to the pressure difference. When 2.8 ml of fluid, corresponding to a filling ratio of 0.65, are inside the PHP, the filling valve is closed.

b) Test protocol and primary operations:

1) A picture of the adiabatic section at time $t = 0$ s is taken.
2) The temperature and pressure signal acquisition system is enabled.
3) The power supply voltage is increased in order to provide the desired amount of heat to the device. The desired heat input level is maintained until a pseudo-steady-state is reached, i.e., until the mean evaporator tube wall temperature achieves constancy). Typical time scales for achieving a steady-state are about 6–10 min; therefore, a given heat input is maintained for about 20 min, before increasing to another power level.
4) Several representative pictures of the flow pattern regimes occurring inside the device are recorded. The temperature profile for the evaporator section, internal fluid temperature and the condenser section are also simultaneously recorded by the DAQ.
5) The heat input level is increased with a step of 10 W.
6) Steps from 2 to 5 are repeated till the maximum heat flux capability is reached. When dry-out state is getting initiated, it is manifested with a decrease in the overall thermal performance of the device; a sharp increase in the evaporator temperature and therefore a corresponding increase in the thermal resistance is noticed. When this state commences, the power supply to the system is stopped for safety reasons.
7) Series of such tests are repeated at different global orientation of the device, from Bottom Heat Mode (i.e. vertical position, with the evaporator zone situated below the condenser) to the horizontal position with steps of 15° in-between.

3. Results and discussion

The input heat power provided to the evaporator zone is one of the key experimental control parameters. Khandekar and Groll [18] showed that the CLPHP may work in different modes (oscillation/circulation) depending on the heat input level and that different flow patterns occur when the heat input is increased. In order to characterize the response to the start-up heat flux, a series of experiments are performed and a common trend has been recognized: for low initial heat input levels (from 0 to 30 W, corresponding to a radial heat flux between 0 and 3.9 W/cm^2) the device behavior is mainly unstable and it cannot reach a pseudo-steady-state even if the heat input is then increased during the experiments; for higher initial heat input levels (from 40 W corresponding to a radial heat flux of 5.2 W/cm^2) the device behavior is much more stable and a pseudo-steady-state of its operation can indeed be reached at each higher heat input level thereafter. For this reason, two sets of experiments are chosen, as representatives of the two situations mentioned above.

- Experiment 1: analysis of the unstable behavior of the PHP for low initial start-up heat inputs;
- Experiment 2: thermo-hydraulics analysis of stable regimes above a critical start-up heat flux.

In both these two tests, the PHP is kept in vertical position with the evaporator zone at the bottom and the condenser at the top (Bottom Heat Mode, BHM).

3.1. Experiment #1: analysis of the unstable behavior

The heat input level is increased with step of 10 W, from an initial heat input level of 20 W. The wall and fluid temperature trends in the left U-turn in the evaporator section are shown in Fig. 5. Different heat input levels are also marked on the time line. Expanded views of these different heat input zones are separately shown in Fig. 6 (20 W zone), Fig. 7 (30 W zone) and Fig. 8 (40 W–50 W zone), respectively.

It is interesting to note that the fluid motion can also be identified and correlated by the oscillation of the fluid temperature; in

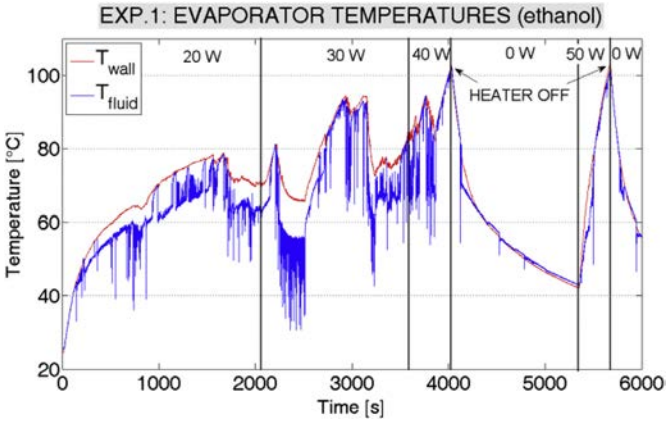

Fig. 5. Experiment #1, temporal evolution of evaporator wall and fluid temperatures, respectively, for different heat inputs.

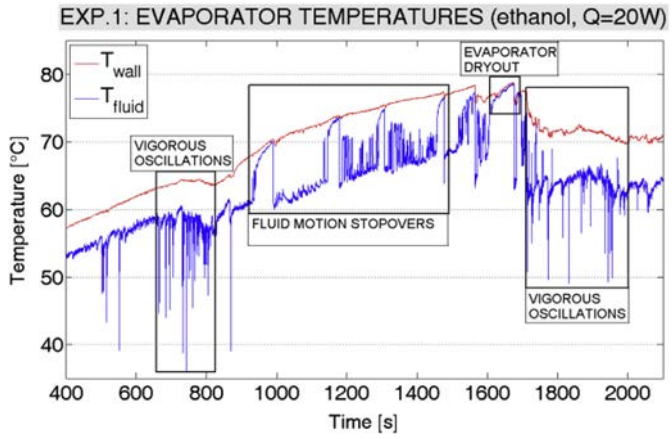

Fig. 6. Experiment #1, temporal evolution of evaporator wall and fluid temperature at 20 W heat input (expanded view of Fig. 5 corresponding to 20 W heat input zone).

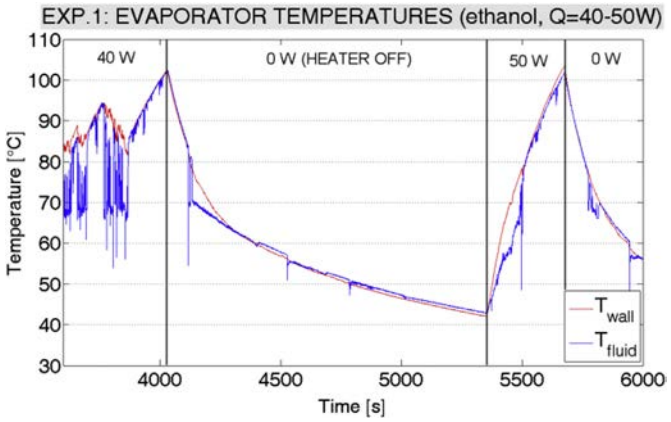

Fig. 8. Experiment #1, temporal evolution of evaporator wall and fluid temperature between 40 W and 50 W heat input (expanded view of Fig. 5 corresponding to 40 W–50 W heat input zone).

particular, the low troughs are related to the passage of a cold liquid slug coming from the condenser section and the higher temperature peaks represent vapor plugs, which are residing in the evaporator U-turns and being heated.

Looking closely on the first heat input period of 20 W (Fig. 6), four different zones are selected, depending on the flow motion. During the start-up (up to 700 s), the fluid motion is very poor and it is mainly due to the merging of the smaller vapor plugs; slug flow with a small oscillation amplitude is present in all branches. As soon as the local fluid temperature reaches ~60 °C and the bigger vapor plugs approach the evaporator, fluid oscillation becomes more vigorous (first box in Fig. 6) and remains stable till the plugs and slugs distribution is unevenly distributed inside the PHP. It is evident that when the oscillation amplitude is larger, the convection is enhanced and the wall cooling is certainly more efficient.

After about 900 s, some big vapor plugs tend to reside in the evaporator section and correspondingly bigger liquid slugs are seen in the condenser. This is a classic meta-stable distribution that damps the fluid oscillations: the vapor plugs positioned in the evaporator are heated up and the PHP heat transfer performance is very low. If fluid temperature and pressure are still relatively low, only a small quantity of colder liquid, in the form of liquid film draining from the hanging liquid plug menisci, is able to reach the evaporator and only a small fluid pulsation is restored. If the slug and plug distribution is again balanced, this stopover phenomenon repeats (second box in Fig. 6) and both wall and fluid temperature keep on rising because of the low heat transfer rate.

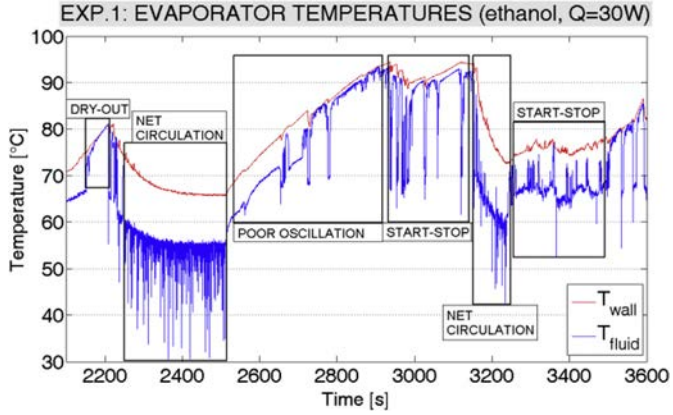

Fig. 7. Experiment #1, temporal evolution of evaporator wall and fluid temperature at 30 W heat input (expanded view of Fig. 5 corresponding to 30 W heat input zone).

As the fluid temperature goes beyond a threshold (between 70 °C and 75 °C) and fluid motion is still poor, all the liquid film surrounding the vapor plugs evaporates and the fluid temperature reaches the wall temperature indicating occurrence of local dry-out (third box in Fig. 6). At this point many different scenarios may occur. At low heat input levels, flow instability may restore an uneven plug and slug distribution and also more vigorous oscillations (fourth box in Fig. 6) may again commence.

At this stage, raising the heat input level from 20 W to 30 W does not lead to a stable behavior and may lead to a new dry-out (see the first box in Fig. 7). Sometimes however, such a condition may also trigger abrupt net circulation of fluid (over and above local oscillations), never present for lower heat inputs. Such a net circulation superimposed on oscillatory flow leads to lower wall temperatures and consequently good heat transfer efficiency (second box in Fig. 7). When the fluid and wall temperatures decrease, the corresponding fluid pressure must also decrease; thus, the net circulation of the fluid cannot be supported anymore. The device starts working somewhat as a heat switch: fluid temperature and pressure rise when fluid oscillations are poor and again decrease, when more vigorous flow motion is activated. Sometimes, as shown in Fig. 8, dry-outs may not evolve at all, at 40 W the poor fluid motion leads to a faster temperature increase and to a consolidation of the inefficient slug and plug motion. The power supply is switched off and again switched on at 50 W but the previous even distribution lead to another occurrence of a fast local dry-out.

The impossibility of getting a steady-state and therefore an acceptable stable thermal performance is mainly due to the simple geometry (only two turns) of the present test-rig. It may also happen that the even distribution of vapour in the evaporator section and liquid in the condenser established after a dry-out event inhibits the subsequent smooth operation even with a boost start-up power input (Fig. 8). It has been well documented that such unstable behavior can be mitigated or even eliminated completely by increasing the number of U-turns [4,5,19,22]. By doing this, the number of heated and cooled section, as well as the local pressure fluctuations due to bends and turns increase, leading to an inherent increase in the internal level of perturbations. The present results substantiate these indications available in the literature and it can be concluded that low number of turns must be avoided for practical applications. This leads to an intrinsic higher probability of liquid slug break-ups and uneven distribution of plugs and slugs, which indeed is the desired pre-requisite of stable thermal performance of a PHP.

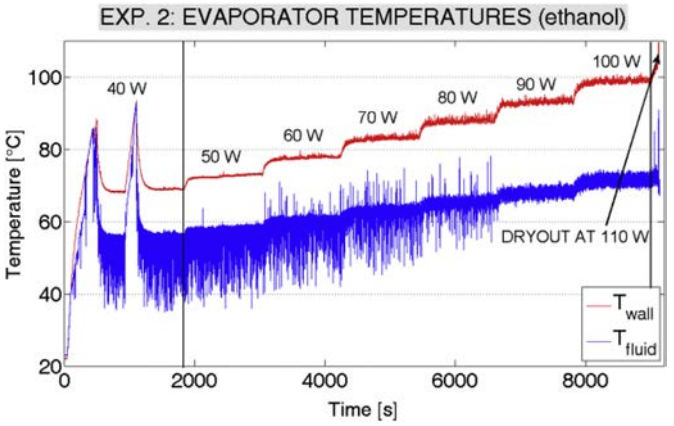

Fig. 9. Experiment #2, temporal variation of evaporator wall and fluid temperatures.

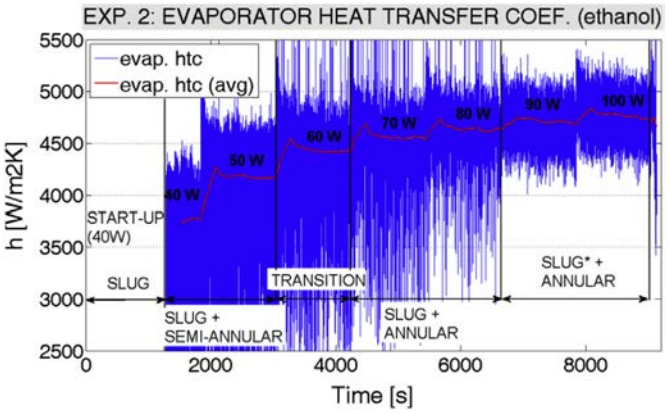

Fig. 11. Experiment #2, temporal evolution of local heat transfer coefficient in the evaporator tube and corresponding internal flow regimes occurring in the device, at different heat inputs.

3.2. Experiment #2: analysis of the stable regimes

As has been pointed out earlier, Experiment #2 corresponds to those runs wherein stable operating regimes of the device were always obtained by providing a start-up heat flux above a critical value. In other words, heat flux increment to the system did not commence with nullity but a minimum value of approximately 5 W/cm^2. This, in turn, ensured satisfactory and stable performance throughout the subsequent increase in heat flux, until a final dry-out was observed.

3.2.1. Wall and fluid temperatures at different heat input levels

The heat input level is increased with step of 10 W, from an initial heat input level of 40 W ($q'' = 5.2$ W/cm^2) to ensure satisfactory operation. Fig. 9 shows the temporal variation of the wall and fluid temperatures, respectively, in the evaporator zone. Indeed, even if at 40 W ($q'' = 5.2$ W/cm^2), the device still tends to operate in the 'Heat Switch Mode', as described for Experiment #1; from 50 W to 100 W ($q'' = 6.5$ W/cm^2–13.0 W/cm^2), net circulating flow is definitely dominant in the PHP, over and above the local oscillations, and the heat transfer operation continues without specific indication of any event which may lead to sudden drop and/or decrease in the device performance. Whenever a step change in input heat flux is done, the new heat input level is kept for at least 20 min so as to ensure that a pseudo-steady-state is reached, as detailed in Fig. 10. The transient period typically lasts for a few hundred seconds, which is essentially attributed to the large thermal inertia of the evaporator plate. It was observed that the present design of the PHP could dissipate up to about 100 W, maintaining the average evaporator wall temperature below 100 °C. Thereafter, clear signs of local dry-outs in the evaporator were observed, as seen in Fig. 9 (at 110 W).

3.2.2. Local heat transfer coefficient and overall performance

Local heat transfer coefficient, as defined below by Eq. (1), is determined after ensuring that a pseudo-steady-state has been reached in the device operation.

$$\tilde{h}_{ev} = \frac{\dot{Q}}{A_{ev} \cdot \left(\Delta T_{w-f}\right)} \tag{1}$$

where ΔT_{w-f}, is the difference between the wall and fluid temperatures, as plotted in Fig. 9, A_{ev} is the evaporator heat exchange area (i.e. inner tube wall surface in the evaporator zone) and $\dot{Q}$ is the input heat power. The local heat transfer coefficient in the evaporator zone (blue line) and its moving average (red line) are shown in Fig. 11. The plot also corresponds to the five different flow patterns, which are recognized during the PHP operation and captured by the camera. Flow regimes are described in detail in the next section.

In order to appreciate the overall performance of such device, the overall thermal conductivity is calculated as follows:

$$k_{eq} = \frac{L_{tot}}{A_{cr}} \frac{\dot{Q}}{\left(T_{w,\max} - T_{\infty}\right)} \tag{2}$$

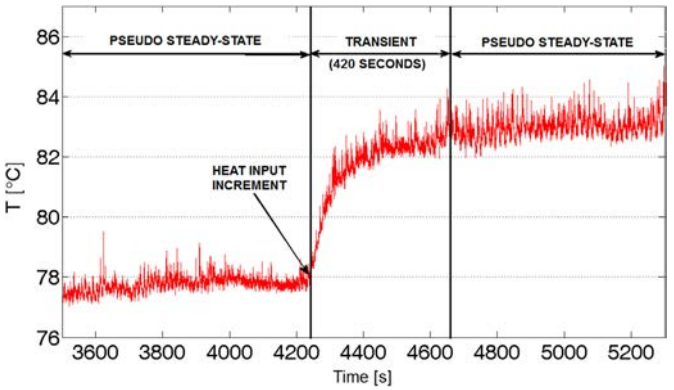

Fig. 10. Typical transient behavior of the evaporator temperature when a step change in heat input is given to the test-rig.

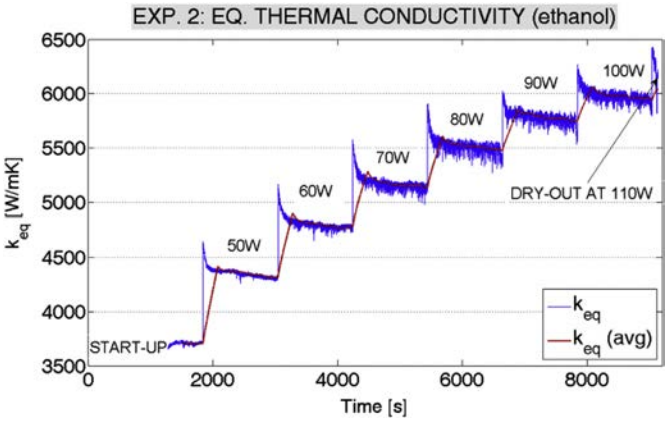

Fig. 12. Experiment #2, temporal variation of equivalent thermal conductivity of the PHP for increasing heat input level.

Table 1
Equivalent thermal conductivity and enhancement factors for different PHPs.

Author/Group	Material/Support	L_{tot} [m]	n [−]	A_{cr} [m^2]	$\dot{Q}_{max}$ [W]	ΔT_{w-c} [K]	k_{eq} [W/m K]	EF [−]	R_{eq} [K/W]
Akachi [3]	Copper/Tube $d_{out} = 3$ mm	0.46	160	0.00113	2000	90	9038	22.6	0.045
Yang et al. [16]	Copper/Tube $d_{out} = 3$ mm	0.12	40	0.00028	400	123	1380	3.4	0.3075
Yang et al. [25]	Aluminium/Plate	0.18	66	0.00036	400	75	2666	10.6	0.1875
Lin et al. [26]	PDMS/Plate	0.06	12	0.00112	8	80	5	29.0	8.0
PHP (this study)	Copper/Tube $d_{out} = 4$ mm	0.2	4	5e−5	100	84	5920	14.8	0.84

where, $A_{cr} = n \cdot \pi \cdot d_{out}^2/4$ is the total PHP cross-section area, L_{tot} is the distance between the hot source and the cooling one, $T_{w,max}$ is the maximum wall temperature (hot side) and T_∞ is the cooling medium temperature (cold side). When a net circulation occurs, the overall thermal conductivity is comprised between 4310 W/m K and 5920 W/m K which means that the device is working from 11 to 15 times better than pure copper (Fig. 12). The overall thermal resistance is estimated as follows:

$$R_{eq} = \frac{(T_{w,max} - T_\infty)}{\dot{Q}} \tag{3}$$

This value can be easily compared with the thermal conductivity of the substrate material by defining an enhancement factor $EF = k_{eq}/k_s$. Table 1 shows the comparison with values extrapolated from other test-rigs in literature: in spite of its simple geometry the present PHP shows quite an appealing performance.

3.3. Flow pattern visualization

A set of images is recorded in order to capture the different flow patterns corresponding to different operating conditions. These, in conjunction with the temperature data, as described earlier, provide important insights into the thermal-hydraulic behaviour of the system.

During the start-up phase the flow pattern is completely slug in all the four branches and the flow is mainly oscillatory in nature, as shown in Fig. 13. This stage is typically characterized by merging of the smaller vapor plugs and formation of bigger ones.

When the heat input level is between 40 W and 50 W, net flow circulation becomes a regular feature getting superimposed on the oscillatory flow. Such bulk circulation is not present at lower heat fluxes. If a vapor plug, coming from the down-comer, is passing through the heated section (i.e., left evaporator U-turn), the liquid film surrounding it evaporates into the vapor plug. The resulting vapor pressure becomes strong enough to push the adjacent liquid slug through the adjacent branch (which acts as the up-header) up to the condenser section. This is exactly what is happening in the second branch of Fig. 14, where a liquid slug is being pushed against gravity by the vapour expansion occurring in the left evaporator U-turn. Due to the circulatory flow, the average volumetric vapor fraction of the up-header is always larger than the average volumetric vapor fraction of the down-comers. As can be clearly seen in Fig. 14, the first and third branches are always pure slug down-comer and the second and fourth branches are characterized by a semi-annular flow pattern, consisting of long annular periods alternated with some occasional transits of the liquid slugs. Due to symmetry, the same phenomena are also happening in the third and fourth branches. As the device is closed in a loop, the vapor pressure in the last branch pushes the fluid up to the condenser and then again down in the first branch (flow direction is explicitly shown in Fig. 14). Thus, owing to a well-defined flow circulation, a sufficient amount of liquid, may be in the form of liquid slugs or in the form of a thin liquid film surrounding each vapour plug, is always available in the evaporator section.

When the heat input level goes up to 60 W (Fig. 15) a flow pattern transition occurs in the two up-comers. The vapour pressure, and the resulting inertia force thereof, in the evaporator section, is now able to break most of the liquid slug menisci bridges and therefore the flow pattern in the two up-comers is changing from semi-annular to pure annular. The liquid film is thick and wavy and a higher amount of the heat transfer is due to the latent heat of vaporization; a 6% gain of the local heat transfer coefficient is recorded with respect to the previous heat input level.

When the heat input level is augmented to 70 W (Fig. 16) and then to 80 W the fluid, which is going up through the second and third branch, has reached the fully annular flow pattern. The liquid film is thinner and less surface waviness is recorded. The augmentation in the value of local heat transfer coefficient is rather low with respect to the previous cases, confirming the fact that

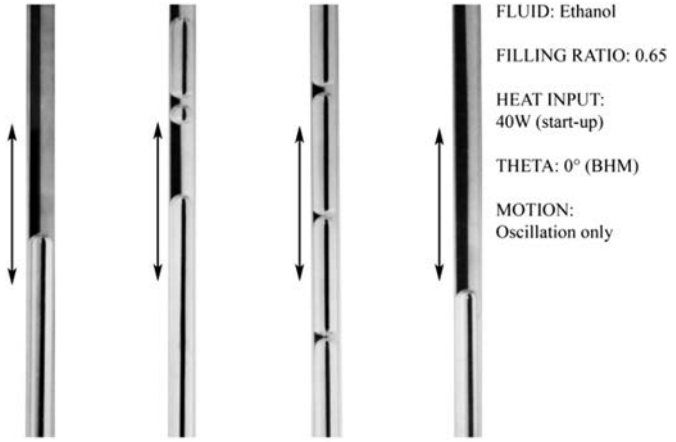

Fig. 13. Experiment #2, flow pattern during the start-up period (SLUG FLOW).

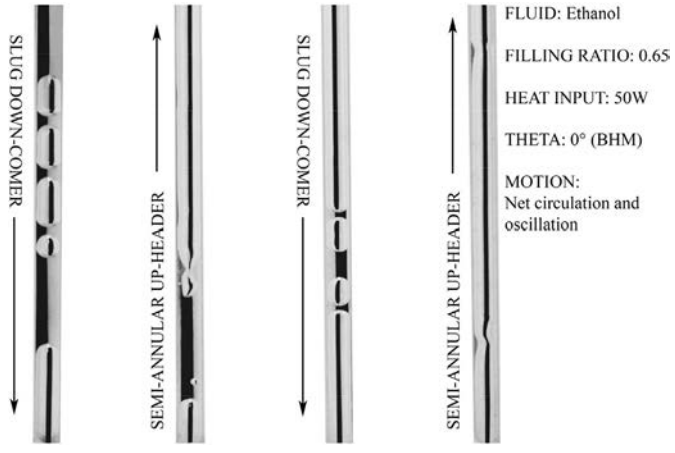

Fig. 14. Experiment #2, flow pattern during the pseudo-steady-state at 40 W–50 W (SLUG + SEMI-ANNULAR).

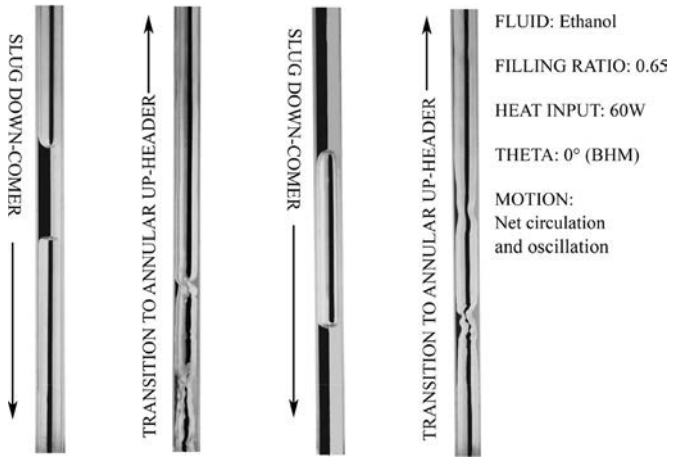

Fig. 15. Experiment #2, flow pattern during the pseudo-steady-state at 60 W (TRANSITION from semi-annular to annular up-comers).

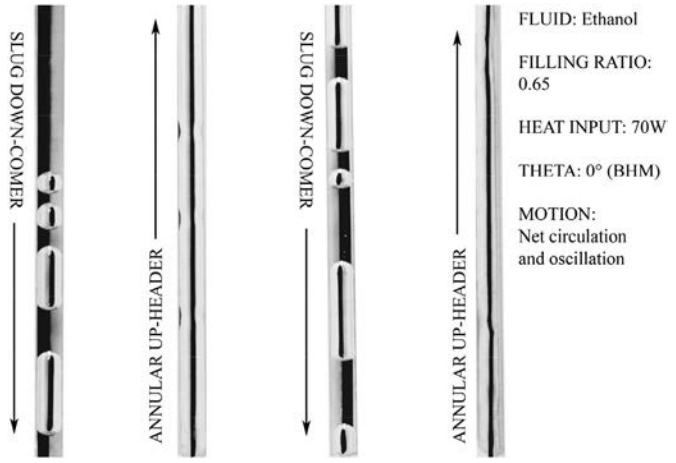

Fig. 16. Experiment #2, flow pattern during the pseudo-steady-state at 70 W (SLUG + ANNULAR).

most of the local heat transfer is due to latent heat and the system is about to reach its maximum heat transfer potential.

Finally, the last two stable pseudo-steady-states (90 W and 100 W) are again characterized by annular up-comers and slug flow down-comers. In these cases, the liquid film in the two up-comers is very thin and, in spite of the fact that the pressure signal is strongly oscillating (liquid slugs in the third down-comer are getting deformed by the strong oscillations), the fluid temperature in the evaporator is not undergoing large variations: the high heat power is now able to evaporate almost all of the liquid coming from the slug down-comer without any vapor reflux (Fig. 17). The vapor fraction in the up-headers is close to 90% or higher.

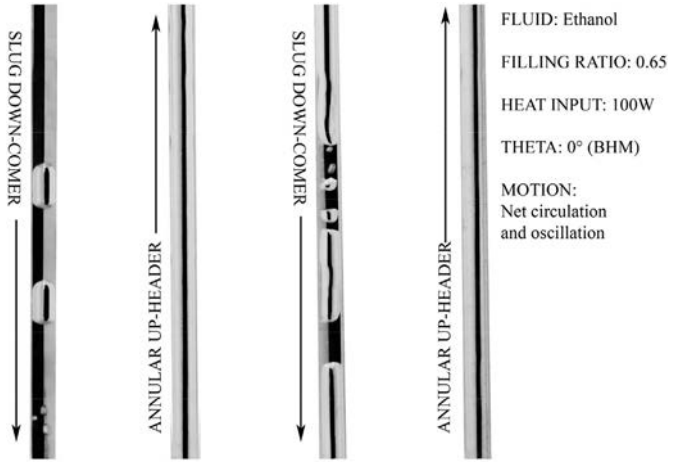

Fig. 17. Experiment #2, flow pattern during the pseudo-steady-state at 100 W heat input level; SLUG (*unstable and non-uniform film thickness) + ANNULAR.

The local heat transfer coefficient is now reaching an asymptotic value and the gain with respect to the previous cases is only around 1%. If the heat input level is increased to 110 W, the slug down-comers are not able to provide a sufficient amount of fresh liquid-phase and an abrupt dry-out occurs in a few minutes.

The flow pattern evolution from pure slug flow to annular flow of the up-comer branches has been often reported in literature [16,18] as a function of the heat input level.

3.4. Pressure signal and its spectral analysis

In order to show that the net fluid circulation is always accompanied by oscillations, the fluid pressure signal over time is plotted in Fig. 18.

During the second pressure ramp at 40 W heat input there are no associated major fluid oscillations (Fig. 18). Therefore, at this

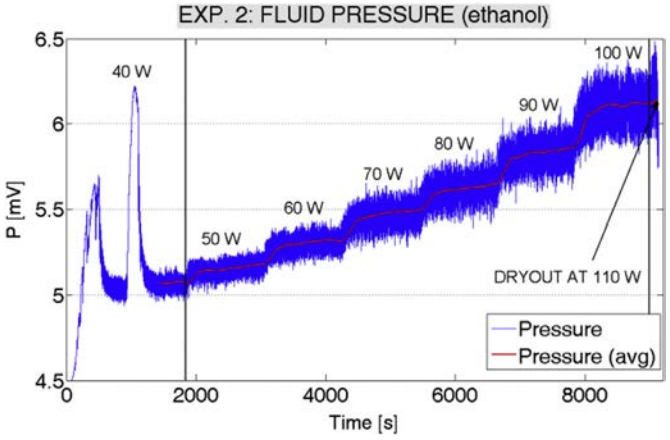

Fig. 18. Experiment #2, temporal evolution of local fluid pressure signal for different heat input levels.

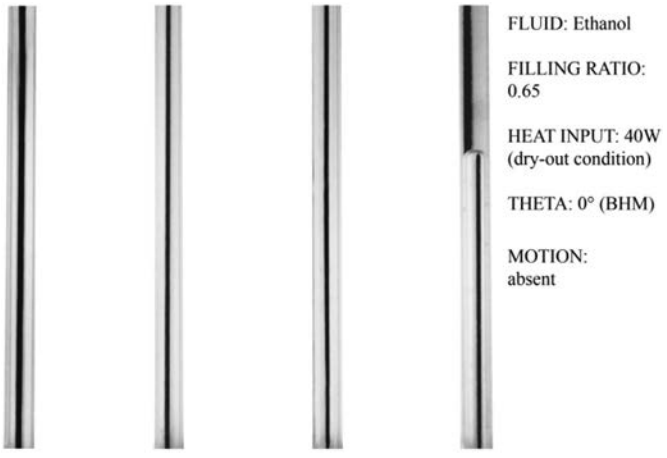

Fig. 19. Experiment #2, local dry-out during the start-up phase.

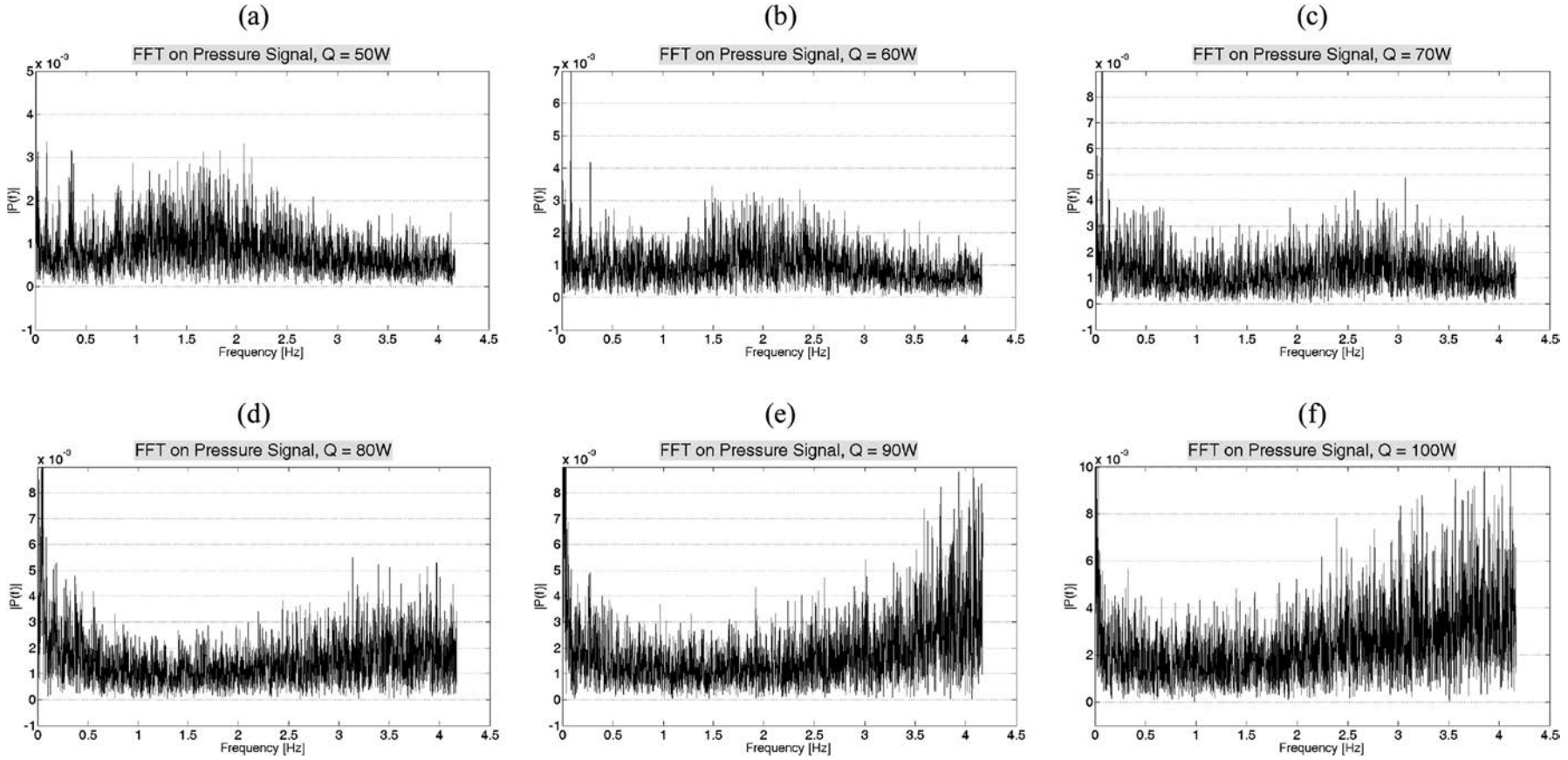

Fig. 20. Fast Fourier Transform of the pressure signal depicting its frequency spectrum at different heat input levels.

point the fluid motion is very poor resulting in a local dry-out condition. The vapour-phase accumulates in the evaporator and the liquid-phase recoils in the condenser section, as confirmed by the visualization study (Fig. 19).

When the fluid circulation is activated, the working fluid average saturation pressure (red line in Fig. 18), as well as amplitude of the fluid pressure oscillation, increases with the heat input level, as also reported by Kim et al. [27]. Since the fluid oscillation is directly connected to the fluid pressure fluctuations, the spectral analysis of pressure signal provides interesting information regarding the existence of dominant or 'characteristic' frequencies. A Fast Fourier Transform with a sampling time of 0.12 s (8.33 Hz) is performed at each heat input level. The sampling frequency is set between 0 and 4 Hz as requested by the Nyquist criterion. As can be seen in Fig. 20, for any of the heat input levels, the oscillating component does not exhibit any regular behaviour in terms of frequency. Kim et al. [27] worked with flat plate geometry with 20 parallel channels and they did not report any fluid net circulation. Their spectral analysis shows distinguishable peaks in the power spectrum comprised between 0.2 and 2 Hz. The value of the dominant frequencies increased with increasing the heat flux and the filling ratio (from 40 vol. % to 60 vol. %). Khandekar et al. [19] performed the same analysis on the single-loop PHP concluding that dominant frequencies of flow oscillations are in the range of 0.1–3.0 Hz with each quasi-steady-state exhibiting a characteristic power spectrum but, looking at the steady-state when their PHP was working with a net circulation, it is also very hard to say what is the fluid oscillation dominant frequency. The authors state that the unidirectional flow circulation corresponds to the best thermal performance, which is inline with the present experimental analysis. It can be safely concluded that the occurrence of fluid circulation is indeed beneficial in terms of improving the thermal performance. In the circulating flow mode an inherent oscillating motion is still present. However, for the present experiments, these pulsations do not exhibit a distinguishable characteristic frequency. This seems to suggest that the increase of thermal efficiency with input heat flux is not directly and fully attributable to the internal flow oscillations. In other words, the data suggests that the enhanced heat transfer is more closely related to the thin film evaporation due to flow transition from slug to annular, which eventually increases the share of the latent heat in the overall heat transfer taking place through the device. These somewhat contradicting trends in the literature regarding the spectral content of the pressure signal and associated exact reasons for enhancement of heat transfer require further scrutiny.

3.5. Effect of tilt angle

The PHP filled with ethanol (constant filling ratio of 0.65 by volume) is tested in six different orientations: from the Bottom Heat Mode (BHM, i.e. vertical position with the evaporator zone situated below the condenser) to the horizontal position, with steps of 15°. For each orientation, the heat input level is increased with step of 10 W, starting from the minimum heat input level which allows a stable behavior, to the maximum heat input level which causes the dry-out of the fluid inside the evaporator zone. Wall and fluid temperature in the evaporator zone, the pressure signal and the different flow patterns in the transparent adiabatic zone, are recorded. The following different flow patterns are recognized:

- S: fully slug flow in all the four branches (unstable behavior);
- SA: semi-annular flow in the two up-comers;
- T: transition from semi-annular to fully annular flow in the two up-comers;
- A: fully annular flow in the two up-comers;
- D: dry-out condition and consequent.

Table 2
Flow patterns for each tilting angle and each heat input level.

Inclination angle	Heat input level [W]										
	10	20	30	40	50	60	70	80	90	100	110
BHM	–	–	–	S	SA	T	A	A	A	A	D
30°	–	–	S	SA	SA	T	A	A	A	A	D
45°	–	S	SA	SA	T	A	A	A	D	–	–
60°	–	S	SA	SA	T	A	A	D	–	–	–
75°	S	SA	SA	T	A	D	–	–	–	–	–
H	–	–	–	–	–	–	–	–	–	–	–

The flow patterns occurring inside the PHP for each tilting angle and each heat input level are noted in Table 2.

It is noticeable that every orientation has its own characteristics, in terms of start-up heat input level: the heat flux needed to activate the fluid motion is also a function of the tilting angle (i.e. the gravity level). In addition, the operating range of allowable heat fluxes shrinks and shifts to lower heat power values as the tilting angle increases. The performance of PHP with such a simple geometry is heavily affected by the inclination with respect to gravity (Fig. 21); indeed the device is not operating at all in the horizontal position. It has been pointed out in the literature that a minimum number of turns coupled with a minimum start-up heat flux are required for the operation of the device to be independent of global orientation [4,5,19,21,24].

For further clarifying the thermal fluid characteristics of the device, the average value of the evaporator wall temperature (Fig. 21), the local mean heat transfer coefficient (Fig. 22) and the equivalent thermal conductivity (Fig. 23), at each heat input level are plotted, for three orientations respectively, BHM, 30° and 60°. The PHP tilted with an angle of 30° works at slightly higher temperatures resulting in a slightly lower equivalent thermal conductivity but the heat input working range is wider: the stable behavior is achievable at 40 W.

Increasing the inclination to 60°, fluid motion gets lesser support of gravity and its motion is less vigorous, resulting in poorer convective heat transfer, as shown in Fig. 22. The heat flux capability is lower (30 W–70 W) but interestingly the device operation is stable at lower heat input levels.

Undoubtedly, one of the critical requirements of a reliable and efficient heat transfer device is orientation independent operation. Increase the number of turns and maintaining the start-up heat flux may help in achieving this target. Reduction in diameter to enhance the surface tension forces is also another solution; however it

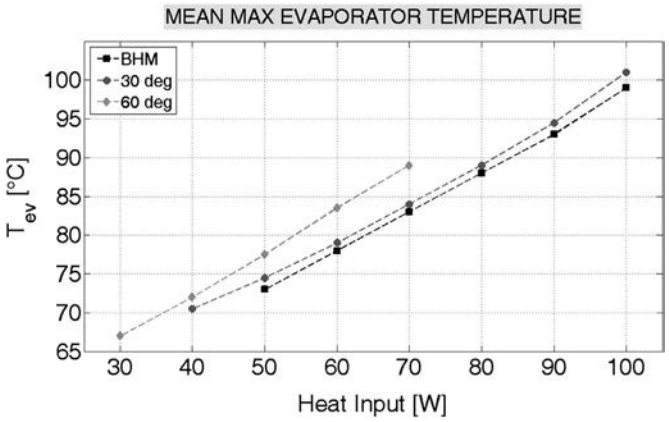

Fig. 21. Maximum mean evaporator temperature for tilting angles equal to BHM, 30° and 60°.

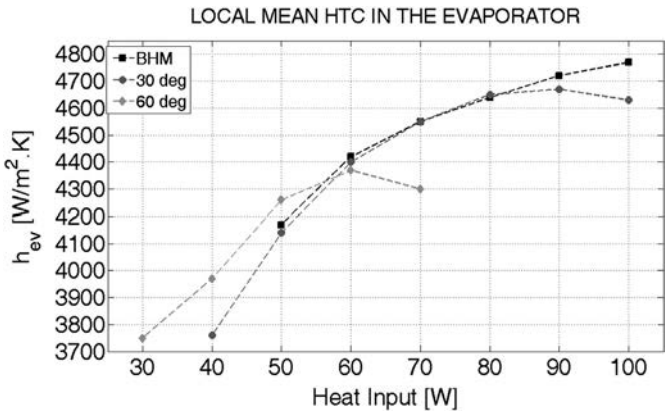

Fig. 22. Local heat transfer coefficient in the evaporator section of the PHP for tilting angles equal to BHM, 30° and 60°, respectively.

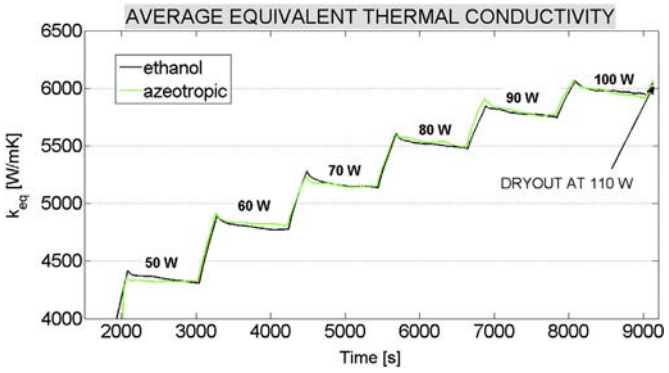

Fig. 24. Comparison of equivalent thermal conductivity of the PHP filled with ethanol and azeotropic mixture of ethanol and water, at different input heat power.

comes at the cost of more pressure drop, thus requiring higher operating heat fluxes. While broad outlines are available in the literature, a systematic parametric assessment on ways of maintaining annular flow in the up-header and slug flow in the down-comer in a multi-turn CLPHP is required as a future work.

3.6. Azeotropic mixture of ethanol–water

Flow boiling of binary mixtures is inherently more complicated than the pure fluid counterpart since the composite thermo-physical properties of the real mixture may substantially differ from those determined from linear mixing laws. The interfacial contact angle of the mixture liquid with the wall, an important quantity required for understanding boiling mechanism, usually shows highly non-linear behaviors with varying mixture concentration. Very limited number of experimental studies on flow boiling of binary mixtures in mini- and micro-channels exist. Furthermore, no explicit heat transfer equation and flow pattern studies are available for binary mixtures, especially of ethanol–water mixtures. Of particular interest is the ethanol–water azeotrope (respectively ethanol 95.5% and water 4.5% by weight) as it has a fixed boiling point of 78.2 °C (at 1 atm), while pure ethanol and pure water boil respectively at 78.4 °C and 100 °C.

Fig. 24 shows the temporal trend of the equivalent thermal conductivity calculated by means of Eq. (2) for the PHP operated with pure ethanol (black line) and the PHP charged with the azeotrope (green line), both in bottom heat mode operation. As is noticeable, no substantial difference in their behaviour is recorded. While this is preliminary data, it will certainly be of interest to check the applicability of low volatility aqueous mixtures, which take the advantage of high latent heat of water but a large (dP/dT) of the low volatility component [28]. Also, the boiling point can be controlled by controlling respective mole fractions, thereby tuning the thermal switch mode of operation. This work is ongoing and will be reported separately.

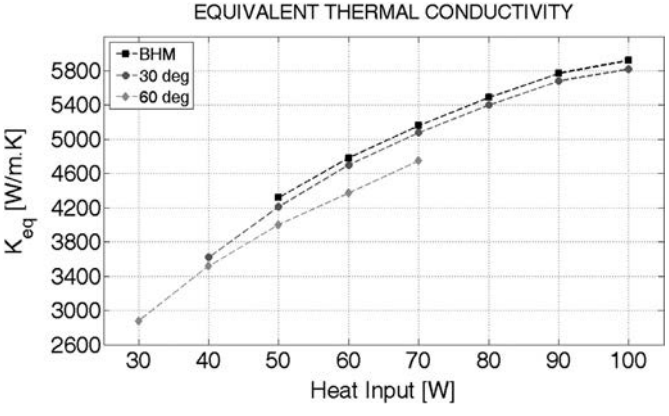

Fig. 23. Overall equivalent thermal conductivity of the PHP as a function of global orientation of the device – BHM, 30° and 60°, respectively.

4. Conclusions

A novel concept of closed loop PHP test-rig has been designed and built in order to perform complete thermal-hydraulic investigation. The fluid pressure and the fluid and wall temperatures are recorded while the flow pattern regime is captured through the transparent adiabatic section. The effects on the device thermal performances of crucial parameters such as the heat input level, the inclination angle and the working fluid are investigated. The local heat transfer coefficient in the evaporator has been measured in a PHP for the first time, at different operating conditions. This information, in conjunction with other measured parameters provides new insights in the passive, self-sustaining, thermally driven two-phase flow boiling process. Finally, the frequency analysis on the fluid pressure signal is performed. The main outcomes of the study are as follows:

- A minimum heat flux is needed to initiate stable fluid motion and reach pseudo-steady-state for each orientation of the device.
- When a stable quasi-steady-state is reached, a net circulation, together with a superimposed oscillating motion, is always recognizable at each heat input level.
- The flow pattern regime in the up-header branches changes from pure slug flow to annular flow by increasing the heat input level. The volumetric concentration of vapor in the up-header is always higher than the down-comer branches.
- The local time-averaged heat transfer coefficient in the evaporator zone has been estimated and related to the different flow patterns. For the present PHP test system approaches an asymptotic value around 4600 W/m^2 K, before the final dry-out occurs.
- Even though the present PHP has a very simple geometry (only two turns), its overall effective thermal conductivity can reach nearly 6000 W/m K, which is a very attractive and impressive value for many practical applications.

- The occurrence of fluid net circulation is beneficial in terms of thermal performance. In the circulating flow mode too, the oscillating motion is still present. However, the spectrum of the pressure signal indicates that it does not exhibit a distinguishable characteristic frequency. Thus, the enhancement of thermal efficiency does not seem to be attributable to specific or characteristic flow oscillations. This aspect certainly requires further research and understanding.
- The performance of PHP with such a simple geometry, especially the low number of turns, is heavily affected by the inclination of the device with respect to gravity. Every orientation has its own stable operating range in terms of heat input level. There is considerable degradation of thermal performance as the device orientation is changed from bottom heat mode to horizontal operation. The device does not operate in the horizontal position.
- In terms of overall thermal resistance, no measurable difference has been recorded between the PHP running with the azeotropic mixture of ethanol–water, as compared to the case it is operating with pure ethanol. However, this topic is an open for further scrutiny.

Acknowledgments

The present work has been carried out at the Indian Institute of Technology Kanpur, India in the framework of the Italian project PRIN2009, which supported the doctoral studies of Mauro Mameli. Partial financial support for conducting the experiments was provided by Bhabha Atomic Research, Department of Atomic Energy, India.

References

[1] G.F. Smyrnov, G.A. Savchenkov, 1971. USSR patent 504065.
[2] H. Akachi, 1990. Structure of a heat pipe. US Patent 4921041.
[3] H. Akachi, 1993. Structure of micro-heat pipe. US Patent 5219020.
[4] L.L. Vasiliev, Heat pipes in modern heat exchangers, Applied Thermal Engineering 25 (2005) 1–19.
[5] S. Khandekar, Thermo-hydrodynamics of Closed Loop Pulsating Heat Pipes. Doctoral dissertation, Universität Stuttgart, Germany, 2004. Available at: http://elib.uni-stuttgart.de/opus/volltexte/2004/1939/ (accessed 01.13).
[6] Y. Miyazaki, Cooling of notebook PCs by flexible oscillating heat pipes, in: Proceedings of ASME InterPACK Conference, San Francesco, USA, 2005. pp. 1–5.
[7] Y. Maydanik, V.I. Dmitrin, V.G. Pastukhov, Compact cooler for electronics on the basis of a pulsating heat pipe, Applied Thermal Engineering 29 (2009) 3511–3517.
[8] S. Rittidech, S. Wannapakne, Experimental study of the performance of a solar collector by closed-end oscillating heat pipe (CEOHP), Applied Thermal Engineering 27 (11–12) (2007) 1978–1985.
[9] M. Arab, M. Soltanieh, M.B. Shafii, Experimental investigation of extra-long pulsating heat pipe application in solar water heaters, Experimental Thermal and Fluid Science 42 (2012) 6–15.
[10] V.S. Nikolayev, A dynamic film model of the pulsating heat pipe, Journal of Heat Transfer, ASME 133 (8) (2011) 081504.
[11] M. Mameli, M. Marengo, S. Zinna, Numerical model of a multi-turn closed loop pulsating heat pipe: effects of the local pressure losses due to meanderings, International Journal of Heat and Mass Transfer 55 (4) (2012) 1036–1047.
[12] S. Maezawa, T. Izumi, K. Gi, Experimental chaos in oscillating capillary tube heat pipes, in: Proceedings of The10th International Heat Pipe Conference, Stuttgart, Germany, 1997.
[13] B. Tong, T.N. Wong, T. Ooi, Closed-loop pulsating heat pipe, Applied Thermal Engineering 21 (18) (2001) 1845–1862.
[14] J.S. Kim, N.H. Bui, J.W. Kim, J.H. Kim, H.S. Jung, Flow visualization of oscillation characteristics of liquid and vapor flow in the oscillating capillary tube heat pipe, Journal of Mechanical Science and Technology 17 (10) (2003) 1507–1519.
[15] P. Charoensawan, S. Khandekar, M. Groll, P. Terdtoon, Closed loop pulsating heat pipes part A: parametric experimental investigations, Applied Thermal Engineering 23 (16) (2003) 2009–2020.
[16] S. Khandekar, P. Charoensawan, M. Groll, P. Terdtoon, Closed loop pulsating heat pipes part B: visualization and semi-empirical modeling, Applied Thermal Engineering 23 (16) (2003) 2021–2033.
[17] S. Khandekar, N. Dollinger, M. Groll, Understanding operational regimes of closed loop pulsating heat pipes: an experimental study, Applied Thermal Engineering 23 (6) (2003) 707–719.
[18] S. Khandekar, M. Groll, An insight into thermo-hydrodynamic coupling in closed loop pulsating heat pipes, International Journal of Thermal Sciences 43 (1) (2004) 13–20.
[19] S. Khandekar, A.P. Gautam, P. Sharma, Multiple quasi-steady states in a closed loop pulsating heat pipe, International Journal of Thermal Sciences 48 (3) (2009) 535–546.
[20] H. Yang, S. Khandekar, M. Groll, Operational limit of closed loop pulsating heat pipes, Applied Thermal Engineering 28 (1) (2008) 49–59.
[21] S. Lips, A. Bensalem, Y. Bertin, V. Ayel, C. Romestant, J. Bonjour, Experimental evidences of distinct heat transfer regimes in pulsating heat pipes (PHP), Applied Thermal Engineering 10 (2010) 900–907.
[22] I. Yoon, C. Wilson, B. Borgmeyer, R.A. Winholtz, H.B. Ma, D.L. Jacobson, D.S. Hussey, Neutron phase-volumetry and temperature observations in an oscillating heat pipe, International Journal of Thermal Sciences 60 (2012) 52–60.
[23] Y. Zhang, A. Faghri, Advances and unsolved issues in pulsating heat pipes, Heat Transfer Engineering 29 (1) (2008) 20–44.
[24] P. Charoensawan, P. Terdtoon, Thermal performance of horizontal closed loop pulsating heat pipes, Applied Thermal Engineering 28 (2008) 460–466.
[25] H. Yang, S. Khandekar, M. Groll, Performance characteristics of pulsating heat pipes as integral thermal spreaders, International Journal of Thermal Sciences 48 (4) (2009) 815–824.
[26] Y.H. Lin, S.W. Kang, T.Y. Wu, Fabrication of poly-dimethylsiloxane (PDMS) pulsating heat pipe, Applied Thermal Engineering 29 (2–3) (2009) 573–580.
[27] H.S. Jung, J.H. Kim, J.W. Kim, J.S. Kim, The study on pressure oscillation and heat transfer characteristics of oscillating capillary tube heat pipe using mixed working fluid, Transactions of the Korean Society of Mechanical Engineers-B 26 (2) (2002) 318–327.
[28] M. Groll, S. Khandekar, Pulsating heat pipes: progress and prospects, in: Proc. 3rd International Conference on Energy and Environment, vol. 1, 2003, pp. 723–730. ISBN 7-5323-7335-5/TK-22, Shanghai, China.